Korean J. Chem. Eng., 35(2), 587-593 (2018)
DOI: 10.1007/s11814-017-0309-5

pISSN: 0256-1115
eISSN: 1975-7220

Mesoporous alumina with high capacity for carbon monoxide adsorption

Changjoo Yeom and Younghun Kim†

Department of Chemical Engineering, Kwangwoon University, 20 Kwangwoon-ro, Nowon-gu, Seoul 01897, Korea
(*Received 23 August 2017 • accepted 5 November 2017*)

Abstract−Carbon monoxide, CO, is an anthropogenic toxic pollutant and its mixture is easily flammable by heated surfaces and open flames. Thus, developing effective adsorbents with a high uptake capacity to adsorb CO from incomplete burned air and flammable gases containing CO is required. Because nanoporous materials are reported to show high performance as adsorbents, we prepared mesoporous alumina (MA) and used it as the CO adsorbent. MA prepared by the post-hydrolysis method showed pore properties such as a uniform pore size, an interlinked pore system, and a large surface area, as compared to commercial adsorbents (activated carbon, zeolite, and silica powder). Adsorption isotherm test was carried out to evaluate the adsorption performance of the as-prepared MA. In addition, Pd-nanodots were immobilized on the MA to enhance the uptake capacity of CO. MA exhibited six to seven-times higher uptake capacity for CO than commercial adsorbents, and its maximum uptake capacity increased 1.3-3.1 times through Pd-nanodots loading. Although the larger surface area of adsorbents is an important factor for ideal adsorbents, a regular and interlinked pore system of adsorbents was found to be more crucial factor to adsorb CO.

Keywords: Nanopore, Mesoporous Alumina, Carbon Monoxide, Adsorbents, Toxic Gases

INTRODUCTION

Carbon monoxide (CO) is a central resource for carbon-based chemical products such as plastics and fibers [1], but is also an anthropogenic toxic pollutant released into the atmosphere [2]. It comes primarily from the incomplete combustion of carbon-containing fuel and engine exhaust fumes in the absence of catalytic converter [3], indicating that it is produced from any burning material. Especially, the flammable mixtures containing CO and other gases can be ignited easily by heated surfaces, open flames, and even by the burning tip of a cigarette. The serious nature of the flammability hazard is reflected in the extensive flammable range of carbon monoxide in air (12.5 to 74%) [4]. When the flammable mixtures of CO are released in chemical accident accompanied by fire, it can easily explode and cause further casualties, because the concentration level of CO that is likely to cause severe health effects is 25 ppm TWA [5]. Therefore, the effective capture of harmful CO from the incomplete burned atmosphere and flammable gases is of great importance both for the protection of secondary damages and health issues.

In recent years, the number of available nanoporous materials, such as metal-organic frameworks (MOFs) [6] and mesoporous silica (MS) [7] as gas adsorbents has increased substantially and emerged as an alternative to zeolite and activated carbon. Because the pore structure and functionality of MOFs and MS can be tailored using structure-directing organic template or surfactant, the porosity of these materials results in high surface areas and uniform porosity, which are key factors to enhance the adsorption capacity of target molecules on the adsorbents. In particular, interest in ordered silica- or alumina-based materials, which are likely to be attractive adsorbents for the removal of pollutants from wastewater and air, has exploded over the past decade [8]. MS has an ideal nanostructure for adsorbents owing to both high specific surface area (200-1,500 m^2/g) and a three-dimensional structure made of highly open spaces, leading to highly porous structures. In various studies of gas adsorption, MS showed very a high uptake capacity and selectivity for CH_4 [9], CO_2 [10], H_2S [11], NH_3 [12], and volatile organic vapors [13]. Although mesoporous alumina (MA) has similar pore properties and high thermal stability as of MS, few studies on the removal of hazardous gases by adsorption using MA have been reported, compared to the reports on MS [14,15]. Therefore, herein, MA was prepared by the post-hydrolysis templating method, and its adsorption capacity for CO gas was evaluated to use it as a high capacity gas-adsorbent in chemical accident accompanied by fire. Since zeolite, activated carbon, and silica nanoparticle have been used as commercial gas-adsorbents in real application fields, these materials were also evaluated for their adsorption capacity for CO. In addition, Pd-nanodot was loaded on the MA to enhance the uptake capacity of CO.

EXPERIMENTAL

1. Preparation of Mesoporous Alumina

Stearic acid and aluminum sec-butoxide were used as the anionic surfactant, and an aluminum precursor was used to prepare MA. As described in our previous reports [16,17], the post-hydrolyzed aluminum precursor produced by the post-hydrolysis method afforded MA with well-organized pore properties such as high surface area and uniform pore distribution. Therefore, the post-hydrolysis method was selected for preparing MA. In brief, the aluminum

†To whom correspondence should be addressed.
E-mail: korea1@kw.ac.kr

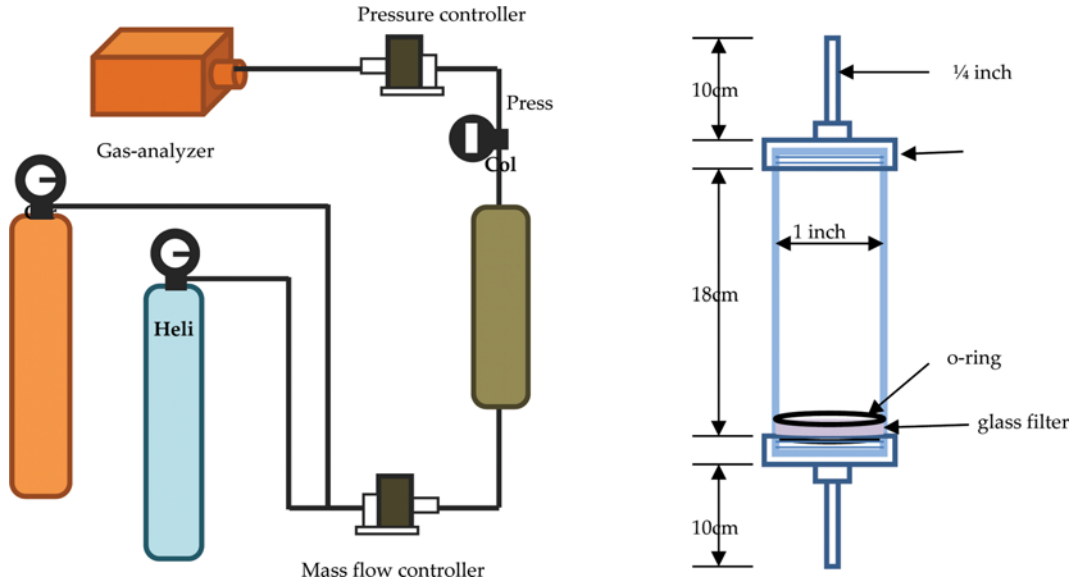

Fig. 1. Experimental system for the adsorption of CO.

precursor and surfactant (stearic acid) were dissolved separately in sec-butyl alcohol, and then the two solutions were mixed. A small amount of water was slowly added dropwise into the mixture at a rate of 1 mL/min generating a white precipitate. This resulting suspension was further stirred for 24 h. The resulting materials were calcined for 3 h at 500 °C in the air. The molar ratio of this reaction mixture was 1 Al(sec-BuO)$_3$: 0.2 $C_{17}H_{35}COOH$: 0.04 NaOH: 5 sec-BuOH: 4 H_2O. In addition, Pd-nanodot supported on adsorbents was prepared by the impregnation method using K_2PdCl_4 as the palladium source. Zeolite (Ze), activated carbon (AC, 100 mesh), and silica (Si, 12 nm) were purchased from Sigma-Aldrich (USA) and used without further treatment as traditional gas-adsorbents.

2. Adsorption of CO

Helium (99.999%) and CO (99.999%) were used as the carrier and target gas, respectively. The experimental setup for measuring isotherm, represented in Fig. 1, consists of a stainless steel column (17 cm length and 2.54 cm inner diameter), with 5 g of packed adsorbent sample, a mass flow controller (max. 5 L/min), a pressure controller (max. 5 bar), and a continuous gas analyzer with a PID-gas detector (GasAlertMicro 5, Honeywell, USA). The concentrations of the mixture of He/CO were adjusted using a gas flow controller. The regeneration conditions were 2 h at 400 °C for all the samples at 5 L/min helium flow. After the regeneration, three recycling tests were carried out for a given pressure. In addition, to define the Gibbs free energy for the adsorption of CO on Pd/MA, the temperature of the reactor was changed from 25 to 50 °C.

3. Characterizations

The porosity of the adsorbents was analyzed by transmission electron microscopy (TEM, JEM-2010, Jeol, Japan). N_2 adsorption/desorption experiments were carried out using a BELSORP-mini (BEL, Japan), and pore size distributions were calculated using the Barrett-Joyner-Halenda (BJH) model on the desorption branch. To analyze the crystallinity, powder X-ray diffraction (XRD, D8 Advance, Bruker, Germany) patterns were recorded using CuKα radiation at 50 kV and 100 mA.

RESULTS AND DISCUSSION

1. Characterizations of Adsorbents

In previous studies [16,18], MA prepared using the chemical template (stearic acid) showed a high adsorption capacity for metal ions (Hg^{2+}, Pb^{2+}, and As^{3+}) from aqueous phase. We found that the surface area of the adsorbents dose not significantly affect the adsorption capacity, and in fact the key factor is a uniform pore size and an interlinked pore system. Since those particle's properties of MA enhanced the adsorption capacity for the removal of metal ions, MA might also be helpful as gas-adsorbent. Since the hydrolysis reaction of aluminum alkoxide in aqueous medium has also led to the formation of lamellar hydrated hydroxides even in the presence of a surfactant molecule, alkyl carboxylate as the surfactant was applied to facilitate the preparation of MA using the post-

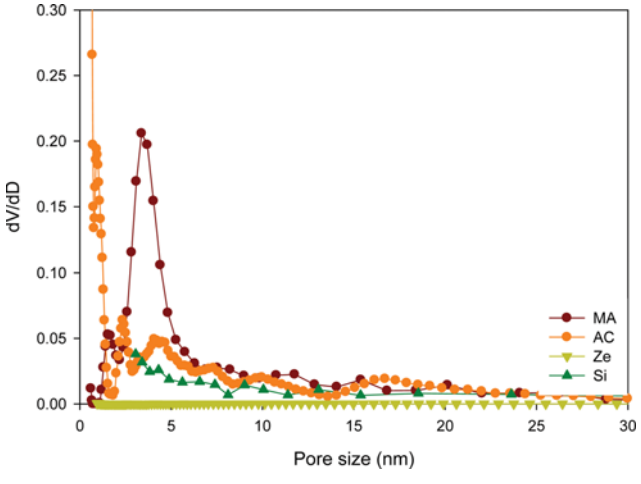

Fig. 2. Pore size distribution of 4 adsorbents, calculated by the BJH model of the desorption branch of the N_2 adsorption/desorption test.

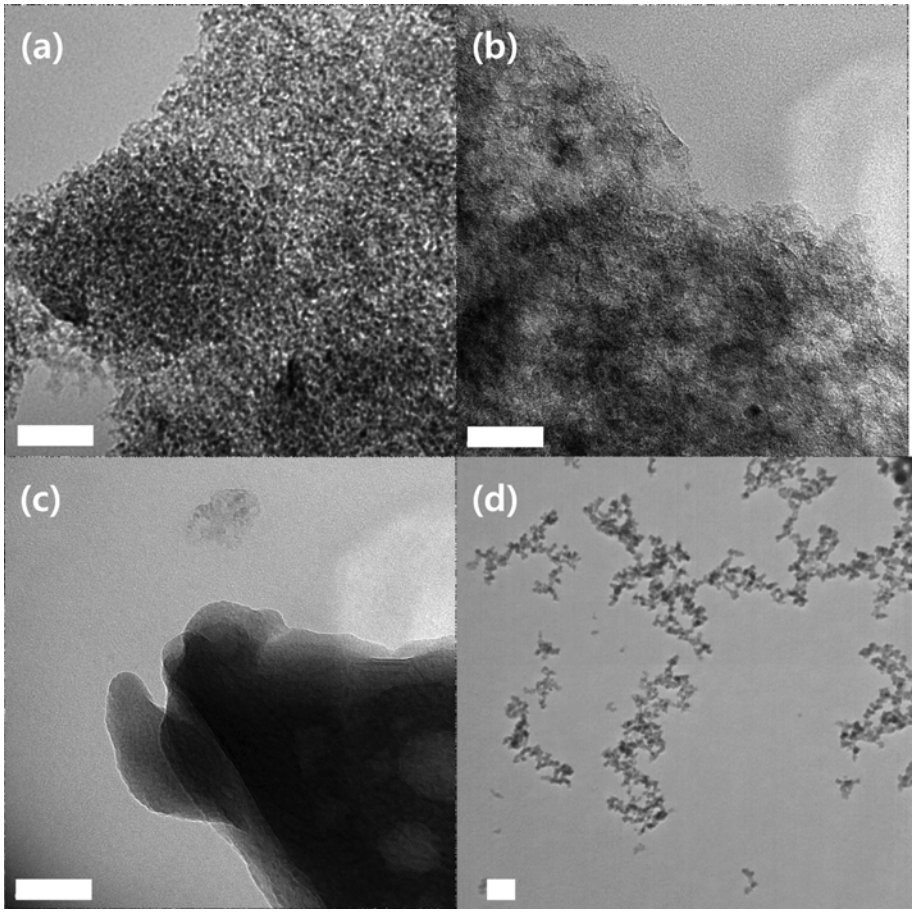

Fig. 3. TEM images of (a) MA, (b) AC, (c) Ze, and (d) Si (1 bar=50 nm).

hydrolysis method. As shown in Fig. 2, MA has nanosized pore diameter (3.4 nm) with a narrow and uniform pore size distribution (D_{FWHM}~2 nm). In N_2 adsorption/desorption isotherm of MA, a typical type of IV isotherm of mesoporous porosity and hysteresis loop in the range 0.4-0.8 P/P_0 was observed, showing both the framework and textural porosity. The framework porosity was in the range 0.4-0.7 P/P_o, indicating that the porosity is contained within the uniform channels of the templated framework, whereas the textural porosity in the range 0.8-1 P/P_o is indicative of the porosity arising from the non-crystalline intra-aggregate voids and spaces formed by interparticle contacts [16]. The TEM images (Fig. 3(a)) of MA show a sponge-like porous appearance and an interlinked pore system [17-19], consistent with the analysis for N_2 adsorption/desorption result of MA. The similar pore morphology was found for disordered mesoporous silica (HMS type) and alumina, when ionic or neutral surfactants were used for their preparation [19]. An interconnected pore structure has an advantage of a reduced diffusion limitation and an enhanced molecular accessibility to the inner surface.

However, other adsorbents (AC, Ze, and Si samples) showed irregular and broad pore size distribution as shown in Fig. 2. The AC sample has a very broad pore distribution in the range 1-25 nm and has a small pore at the inner surface and large surface area (1,024.2 m^2/g), but the non-uniform pore structure does not match with the physical properties of ideal adsorbents. Nevertheless, it is inexpensive and has a large surface area, so it is widely used as a commercial adsorbent. Therefore, herein, AC was selected as the reference material to MA. Molecular sieve such as Ze sample has generally very small pore (2-10 Å), which is suitable feature for size-selective separation of small molecules. Since the pore size of Ze is too small to be measured by N_2 adsorption/desorption test, their pore size was not calculated by the BJH model (the bottom line in Fig. 2). As shown in Fig. 3(c), the morphology of Ze sample shows a solid yet smooth surface. Although Si sample has a single particulate form with 12 nm size, the TEM image of the Si sample shows an aggregated form between single particles (Fig. 3(d)). Because

Table 1. Pore properties of the samples

Samples	Surface area (m^2/g)	Pore size (nm)	Pore volume (cm^3/g)
MA	334.2	3.39	0.759
AC	1024.2	1 to 25	0.704
Ze	1.9	NA	NA
Si*	365.8	4.92*	1.097*

*Since silica nanoparticles have not porous nanostructure, its pore size and pore volume in table means the void fraction originated from agglomeration or aggregation between primary particles

the void fraction originates from the agglomeration or aggregation between the primary particles, it acts as pores in the N_2 adsorption/desorption test. Thus, the pore size distribution of Si sample was measured, as shown in Fig. 2. The pore properties of all the adsorbents are listed in Table 1.

Several studies of the CO adsorption energy as a function of particle size of Pd supported on Al_2O_3 have appeared in the literature, yielding a key result [20,21]. Namely, smaller particle size of Pd cluster on Al_2O_3 favors a higher CO adsorption energy [20]. In addition, it was reported that the carbonate formation on Pd/Al_2O_3 occurs by oxygen down reaction of CO with the hydroxyl groups on the support [21]. Therefore, herein, Pd was deposited on the MA to induce strong adsorption between CO and Pd/MA. To confirm the Pd loading on the support, the XRD patterns of MA and Pd/MA were compared (Figs. 4(a) and 4(b)). Alumina has a variety of crystalline structures, and MA shows three major peaks in the spinel structure of alumina. The XRD patterns of MA typically show the characteristic peaks of activated γ-Al_2O_3, and Pd/MA has additional peaks for Pd metal at 40 and 82° in the XRD pattern. In addition, after deposition of Pd on the supports, TEM analysis was carried out (Figs. 4(d) and 4(e)). The smaller Pd nanoparticles were immobilized on the MA compared to AC. The crystallite size of Pd nanodots loaded on MA and AC was calculated as 5.9 and 18.4 nm by using the Scherrer equation based on the half-width of the (111) peak, respectively, which was consistent with the TEM result. Notably, MA is a more suitable adsorbent to load Pd-nanodots on their supports owing to its pore uniformity and regular pore size distribution, whereas Ze does not have a suitable pore size to load Pd-nanodots; thus Pd was not loaded on the Ze sample. Since Si sample has an aggregated form, Pd-nanodots synthesized in the aqueous phase also aggregated with the existing Si nanoparticles. Therefore, it was confirmed that Pd-nanodots were only immobilized on the MA and AC samples. RD patterns of MA and Pd/MA typically show the characteristic peaks of the activated adsorbents.

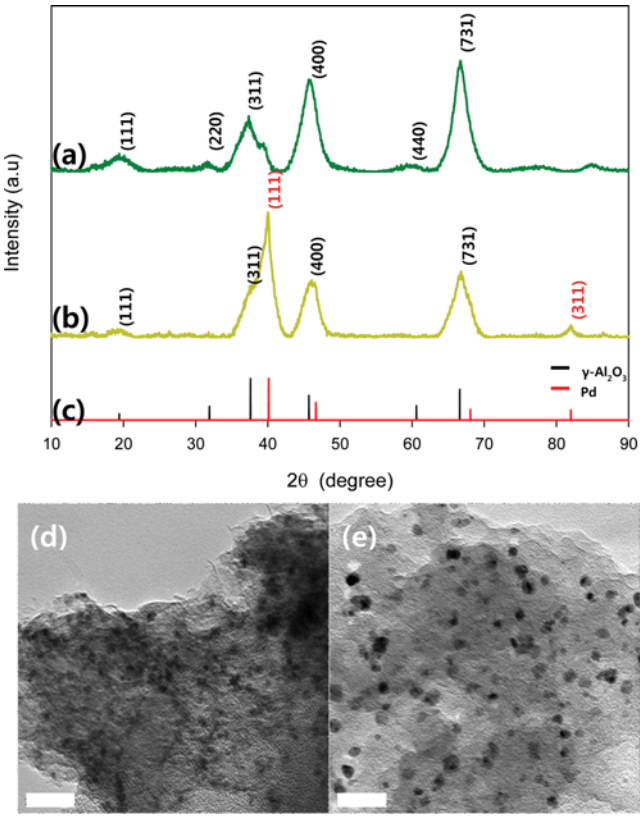

Fig. 4. XRD patterns of (a) MA, (b) Pd/MA, and (c) reference γ-Al_2O_3 (JCPDS 01-076-4179) and Pd (JCPDS 00-005-0681). TEM images of (d) Pd/MA and (e) Pd/AC (1 bar=50 nm).

2. Adsorption Equilibrium Study

To define the maximum adsorption capacity of CO on the adsorbents, it is important to establish the most appropriate correlation for the equilibrium curves. In the case of gas adsorption, pressure is the controlling parameter to enhance the gas uptake on adsorbents. Therefore, with increasing applied pressure of CO gas, their uptake capacity generally increased up to saturation at high pressure. As shown in Fig. 5(a), the uptake of CO gas on MA increased linearly to 2.5 bar and then increased rapidly thereafter. This feature was similar to a typical type V isotherm of water vapor on a porous metal cluster [22]. Namely, CO molecules were first adsorbed on the outer surface of adsorbent at a relatively low pressure and then gradually penetrated into the inner surface of the adsorbent to adsorb at a relatively high pressure.

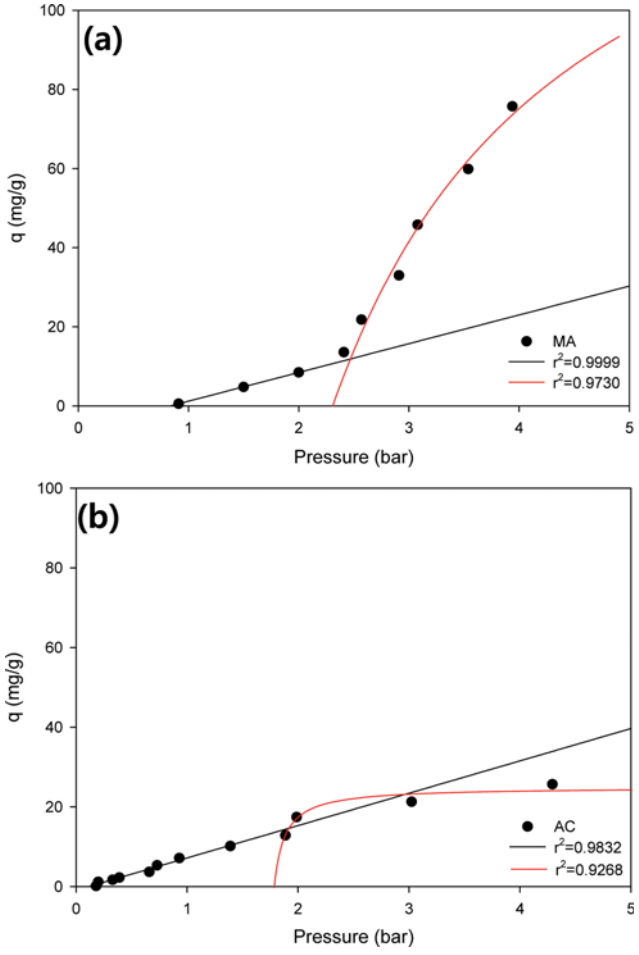

Fig. 5. Isotherms of CO on the (a) MA and (b) AC.

Table 2. Parameters of Langmuir isotherm and adsorption density for CO on MA, AC, Ze and Si

Samples	Q_m (mg/g) at 25 °C	Γ_{max} (mg/m^2) at 25 °C
MA	170.4	0.40
AC	25.2	0.06
Ze	28.3	0.07
Si	26.8	0.06
Pd/MA	228.5	0.53
Pd/AC	77.6	0.18
Pd/Si	34.6	0.08

Since the internal diffusion of CO molecules on the adsorbents was enhanced at a high pressure, the adsorption of CO increased at a relatively high pressure. The deviation of the adsorption isotherm from the ideal Langmuir adsorption, known as significant two-step pressure-dependent adsorption, is because of cooperative adsorption or interactions between the adsorbates for multilayer adsorption [23]. The isotherm of CO on AC also showed a similar adsorption curve with that of MA (Fig. 5(b)). The connection point between the linear adsorption and Langmuir adsorption was found at ca. 2 bar for all the adsorbents.

The Langmuir adsorption isotherms in the high pressure range are plotted in Fig. 5, and the maximum uptake capacities (Q_m, mg/g) for CO were calculated. As summarized in Table 2, the Q_m values of the CO uptake on MA, AC, Ze, and Si adsorbents are 170.4, 25.2, 28.3, and 26.8 mg/g, respectively. Other adsorbents except MA showed a similar high uptake capacity for CO (6.7 times of AC). It is reported that commercial AC and 5A zeolite have adsorption capacity for CO in the range 100-150 mg/g [24]. Therefore, MA used here is referred as a good gas-adsorbent with a very high adsorption capacity for CO. The adsorption density (Γ, mg/m^2) of CO on the active surface of adsorbents was calculated using well-known equation, $V\Delta C/mS$, where S, m, V, and C are the surface area, amount of adsorbent, volume and adsorbed concentration of CO, respectively [16]. The maximum adsorption density (Γ_{max}) was obtained from the adsorption isotherm, and a similar trend with the maximum uptake of CO was observed. Namely, the uptake capacity has almost a linear correlation with the adsorption density; Γ_{max}=0.0023 Q_m+0.0007.

The mechanism of the carbonate formation of CO on Pd/Al_2O_3 can be monitored by infrared spectroscopy [21]. A comparison of CO chemisorption on pristine Al_2O_3 and Pd/Al_2O_3 indicated that ~20% of the adsorbed CO on Pd/Al_2O_3 reacted on the support, when Pd is loaded on the metal oxide support, thus enhancing the CO adsorption. Herein, Pd-nanodots loaded adsorbents (Pd/MA, Pd/AC, and Pd/Si) were also evaluated for their adsorption capacity for CO. As shown in Fig. 6, the CO adsorption with pressure followed the cooperative adsorption. After loading of Pd-nanodots on the adsorbents, their maximum uptake capacity for CO increased. Pd/MA and Pd/AC showed 228.5 and 77.6 mg/g of the maximum capacity of CO, respectively. The affinity of CO molecules to the Pd supported adsorbents was 1.3- and 3.1-folds larger than of the pristine MA and AC, respectively.

Because the adsorption of gas is strongly affected by temperature, the Gibbs energy and the uptake capacity for Pd/MA adsorbent were evaluated at different temperatures (25, 30, and 50 °C). As shown in Fig. 7, the adsorption curve at high temperature was located below that of the room temperature. The maximum capacities of CO at 30 and 50 °C were 172.5 and 126.2 mg/g, respectively, which were lower than those obtained at 25 °C. The Gibbs free energy of the adsorption was calculated (Table 3), and the adsorp-

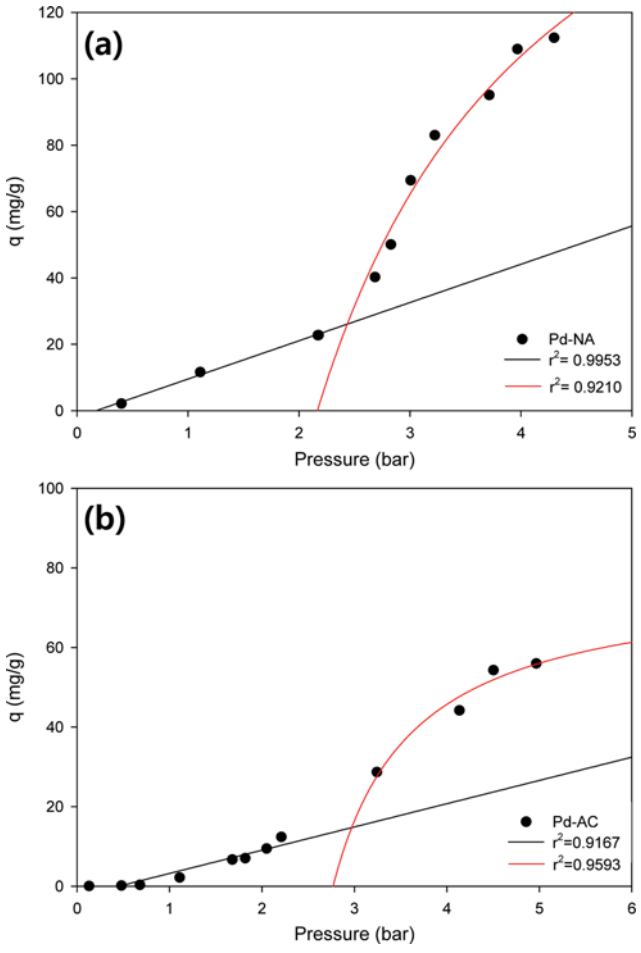

Fig. 6. Isotherms of CO on the (a) Pd/MA and (b) Pd/AC.

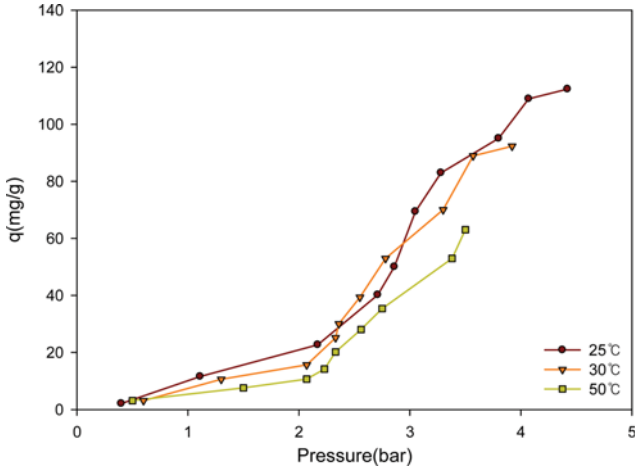

Fig. 7. Isotherms of CO on the Pd/MA at different temperature.

Table 3. Gibbs free energy of CO adsorption on Pd/MA at different temperatures

Temperature	Q_m (mg/g)	$-\Delta G$ (kJ/mol)
25 °C	228.5	14.3
30 °C	172.5	13.8
50 °C	126.2	13.6

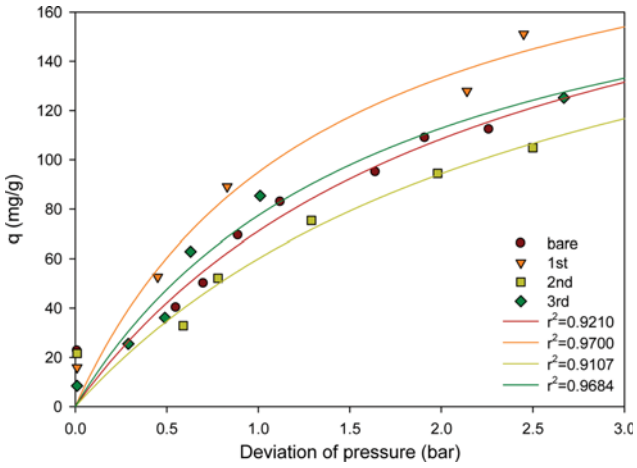

Fig. 8. Isotherms of CO on the Pd/MA with recycling number.

tion energy value (ca. −14 kJ/mol) was similar with the reported data [24]. With increasing temperature, $-\Delta G$ decreased, decreasing the interaction between CO and supports. Therefore, the adsorption system under high temperature poses a negative impact on the adsorption capacity, decreasing the amount of adsorbed gas.

In the field applications of CO adsorbents, maintaining the initial uptake capacity after regeneration is also an important factor for ideal adsorbents. Pd/MA was selected as the model adsorbent for the regeneration test and was regenerated at 400 °C at 5 L/min He flow. After the regeneration, the feasibility of the adsorption-desorption cyclic operation was examined to investigate the repeatability performance of Pd/MA. As shown in Fig. 8, the amount of adsorbed CO changed with the repeated use of adsorbent. While >91% of the initial uptake capacity of Pd/MA was maintained after three cycles of operations, notably Pd/MA can undergo repeated adsorption-desorption cycles without any loss of activity.

3. Effect of Supports and Pd-loading

AC and Ze samples are typically used to remove volatile organic compounds and hazardous gases in house and industry. Herein, several adsorbents (AC, Ze, and Si) with different pore properties were also evaluated for their uptake capacity for CO adsorption. Although AC has a high surface area (1,024.2 m^2/g), it shows a low uptake capacity of 25.2 mg/g CO. Although Si sample has a similar surface area with MA, induced by the formation of aggregates between single silica nanoparticles, Si also shows a low uptake capacity. These results show that the surface area of adsorbents does not significantly affect the adsorption capacity. A common feature of the AC and Si is their irregular pore size distribution. It is noted that ill-defined pore structure reduces the adsorption of CO to adsorbents. In contrast, a uniform pore structure with well-defined channels has been shown to have a great advantage over a disordered pore network in terms of access of guest species to the binding sites [25]. Therefore, the surface area of the adsorbent is likely to be large, but the pore structure (i.e., regular interlinked pore system) is the most important factor for the CO adsorption. The MA adsorbent used in this study has a six- to seven-times higher uptake capacity than those of AC, Ze, and Si samples. In addition, to increase the interaction between the CO and surface of adsorbents, Pd-nanodots were immobilized on the adsorbents, and their uptake capacity was increased. Based on the mechanism of "oxygen down" reaction with the hydroxyl groups on the alumina [21], carbonate formation occurs via the reaction of CO with the surface hydroxyls, followed by instantaneous reaction of CO_2 with the oxide support. Consequently, a regular pore structure (prefer to interlinked pore system) was found to be the most critical factor for the removal of CO using MA. In addition, Pd/MA is the most suitable gas-adsorbent with a high adsorption capacity for CO.

CONCLUSIONS

MA, which was prepared by the post-hydrolysis method using chemical template, was used as the gas adsorbent for high concentration of CO released in chemical accident accompanied by fire. MA adsorbent showed characteristic pore properties such as uniform pore size, regular pore size distribution, interlinked sponge-like pore system, and large surface area of ideal gas-adsorbents. Since MA showed a great applicability in environmental applications for the removal of heavy metal ions and organic pollutants, in this study, it was used as a model adsorbent for the adsorption of CO gas. Pd-nanodots were immobilized on the surface of MA to enhance the uptake capacity of CO on adsorbents, and their CO adsorption performance was compared to commercial gas-adsorbents (activated carbon, zeolite, and silica nanoparticle). This study on the isotherm adsorption represents the significant two-step pressure-dependence, namely, cooperative adsorption, deviated from the ideal Langmuir adsorption. The maximum uptake capacity of CO for MA was 170.4 mg/g and is six- to seven-times larger than the commercial adsorbents, and their capacity enhanced through Pd-nanodot loading on MA (228.5 mg/g for Pd/MA). The correlation between the uptake capacity and pore properties of adsorbents was investigated, and the adsorption performance is not good even if the surface area is large as in the case of AC. The key characteristic of adsorbents that determines the CO adsorption capacity is its uniform pore structure with an interlinked pore system and wide surface area. Consequently, MA and Pd/MA were found to be the most suitable CO gas adsorbents. In addition, because the adsorption energies of the toxic gases and common adsorbates follow the trend NH_3>PH_3>H_2S>SO_2>CO [2], it is possible to apply as-prepared MA readily as conventional gas-adsorbents for NH_3 and PH_3 as well as CO.

ACKNOWLEDGEMENTS

This study was supported by the Research Grant from the Korea Environmental Industry & Technology Institute

(2015001960003) and the National Research Foundation of Korea (2017R1A2B4001829).

REFERENCES

1. H. Sato, W. Kosaka, R. Matsuda, A. Hori, Y. Hijikata, R. V. Belosludov, S. Sakaki, M. Takata and S. Kitagawa, *Science*, **343**, 167 (2014).
2. E. Barea, C. Montoro and J. A. R. Navarro, *Chem. Soc. Rev.*, **43**, 5419 (2014).
3. E. A. Sandilands and D. N. Bateman, *Medicine*, **44**, 151 (2016).
4. *Carbon monoxide in the workplace*, Industrial Accident Prevention Association (2008).
5. *Environmental health criteria 213 Carbon monoxide*, International Programme on Chemical Safety, World Health Organization (1999).
6. T. G. Glover, G. W. Peterson, B. J. Schindler, D. Britt and O. Yaghi, *Chem. Eng. Sci.*, **66**, 163 (2011).
7. S. E. Lehman and S. C. Larsen, *Environ. Sci.: Nano*, **1**, 200 (2014).
8. A. Walcarius and L. Mercier, *J. Mater. Chem.*, **20**, 4478 (2010).
9. W. S. Chiang, E. Fratini, P. Baglioni, J. H. Chen and Y. Liu, *Langmuir*, **6**, 8849 (2016).
10. A. Hanif, S. Dasgupta and A. Nanoti, *Chem. Eng. J.*, **15**, 703 (2015).
11. Y. Belmabkhout, G. D. Weireld and A. Sayari, *Langmuir*, **25**, 13275 (2009).
12. C. Zamani, X. Illa, S. Abdollahzadeh-Ghom, J. R. Morante and A. R. Rodriguez, *Nanoscale Res. Lett.*, **4**, 1303 (2009).
13. C. T. Hung and H. Bai, *Chem. Eng. Sci.*, **63**, 1997 (2008).
14. J. A. Thote, R. V. Chatti, K. S. Iyer, V. Kumar, A. N. Valechha, N. K. Labhsetwar, R. B. Biniwale, M. K. N. Yenkie and S. S. Rayalu, *J. Environ. Sci.*, **24**, 1979 (2012).
15. C. Chen and W. S. Ahn, *Chem. Eng. J.*, **1666**, 646 (2011).
16. Y. Kim, C. Kim, I. Choi, S. Rengaraj and J. Yi, *Environ. Sci. Technol.*, **38**, 924 (2004).
17. Y. Kim, B. Lee and J. Yi, *Korean J. Chem. Eng.*, **24**, 679 (2007).
18. S. Rengaraj, J. W. Yeon, Y. Kim and W. H. Kim, *Ind. Eng. Chem. Res.*, **46**, 2834 (2007).
19. Y. Kim, C. Kim and J. Yi, *Mater. Res. Bull.*, **39**, 2103 (2004).
20. D. R. Raner, M. C. Wu, D. I. Mahon and D. W. Goodman, *J. Vac. Sci. Technol.*, **14**, 1184 (2996).
21. K. Fottinger, R. Schlogl and G. Rupprechter, *Chem. Commun.*, 320 (2008).
22. M. I. H. Mohideen, B. Xiao, P. S. Wheatley, A. C. McKinlay, Y. Li, A. M. Z. Slawin, D. W. Aldous, N. F. Cessford, T. Duren, X. Zhao, R. Gill, K. M. Thomas, J. M. Griffin, S. E. Ashbrook and R. E. Morris, *Nature Chem.*, **3**, 304 (2011).
23. S. Liu, *J. Colloid Interface Sci.*, **450**, 224 (2015).
24. M. Bastos-Neto, A. Moeller, R. Staudt, J. Bohm and R. Glaser, *Sep. Purif. Technol.*, **77**, 251 (2011).
25. Y. Wang, C. Bryan, H. Xu, P. Pohl, Y. Yang and C. J. Brinker, *J. Colloid Interface Sci.*, **254**, 23 (2002).